Materials Advances

ROYAL SOCIETY OF CHEMISTRY

PAPER

View Article Online
View Journal | View Issue

Open Access Article. Published on 26 September 2023. Downloaded on 12/4/2025 9:20:33 PM.
This article is licensed under a Creative Commons Attribution-NonCommercial 3.0 Unported Licence.

Check for updates

Cite this: *Mater. Adv.*, 2023, 4, 5149

Effects of hydrocarbon substituents on highly fluorescent bis(4-phenylphenyl)pyridylmethyl radical derivatives†

Yohei Hattori,*[a] Ryota Kitajima,[a] Atsumi Baba,[a] Kohei Yamamoto,[a] Ryota Matsuoka,[bcd] Tetsuro Kusamoto[bcde] and Kingo Uchida[a]

Received 26th July 2023,
Accepted 21st September 2023

DOI: 10.1039/d3ma00469d

rsc.li/materials-advances

Eight new stable luminescent radicals are reported. We previously reported that the photoluminescence quantum yields (PLQYs) of diphenylpyridylmethyl radicals is dramatically increased by the addition of mesityl (2,4,6-trimethylphenyl) groups. By changing the mesityl groups to other hydrocarbon-substituted phenyl groups, the issue of the fluoresence efficiency and photostability of these radicals could be clarified. Contrary to our expectations, changing 2,4,6-trimethyl to 2,4,6-triisopropyl did not produce a positive effect, other than some improvement in purification. Nevertheless, a PLQY of more than 60% was a significant value. The addition of methyl substituents at the *meta*-positions drastically quenched the fluorescence in dichloromethane, while maintaining bright fluorescence in chloroform. Removing one of the *ortho*-methyl groups somewhat decreased the fluorescence efficiency but greatly improved the photostability. By using a phenyl substituent instead of a methyl group, more stabilization under photoirradiation could be achieved.

Introduction

Recently, stable luminescent radicals have attracted much attention for application in highly efficient OLEDs[1] utilizing their emitting D_1 (doublet lowest excited state) to D_0 (doublet ground state) transition. They are also actively studied as emitting materials closely related to electron spin[2] and magnetism.[3]

Leaving aside the new types of luminescent radicals that are on the rise,[4] polyhalogenated triarylmethyl radicals have established a high degree of stability and a variety of derivative types.[5] The most basic stable luminescent triarylmethyl radicals are triphenylmethyl radicals such as tris(2,4,6-trichlorophenyl)-methyl radical (TTM, Scheme 1)[6] and perchlorotriphenylmethyl radical (PTM),[7] and the second group that is similarly easy to obtain and handle is diphenylpyridylmethyl radicals such as (3,5-dichloro-4-pyridyl)bis(2,4,6-trichlorophenyl)methyl radical (PyBTM)[8] and (3,5-difluoro-4-pyridyl)bis(2,4,6-trichlorophenyl)-methyl radical (F_2PyBTM).[9] PyBTM and F_2PyBTM are superior to TTM in terms of their stability under light irradition[8,9] and unique in their ability to form metal complexes.[10] However, diphenylpyridyl radicals had been less explored than triphenylmethyl radicals for making highly fluorescent derivatives in

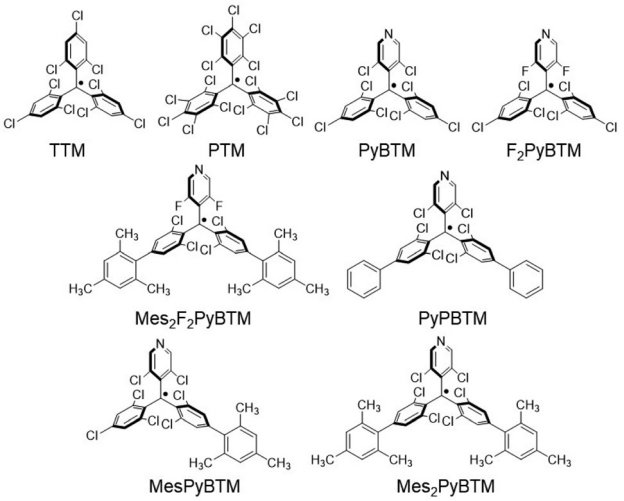

Scheme 1 Structures of TTM and PyBTM derivatives.

[a] Materials Chemistry Course, Faculty of Advanced Science and Technology, Ryukoku University, Seta, Otsu, Shiga 520-2194, Japan. E-mail: hattori@rins.ryukoku.ac.jp
[b] Department of Life and Coordination-Complex Molecular Science, Institute for Molecular Science, 5-1, Higashiyama, Myodaiji, Okazaki, Aichi 444-8787, Japan
[c] SOKENDAI (The Graduate University for Advanced Studies), Shonan Village, Hayama, Kanagawa 240-0193, Japan
[d] Graduate School of Engineering Science, Osaka University, 1-3, Machikaneyama, Toyonaka, Osaka, 560-8531, Japan
[e] JST-PRESTO, 4-1-8, Honcho, Kawaguchi, Saitama 332-0012, Japan

† Electronic supplementary information (ESI) available. See DOI: https://doi.org/10.1039/d3ma00469d

© 2023 The Author(s). Published by the Royal Society of Chemistry

Open Access Article. Published on 26 September 2023. Downloaded on 12/4/2025 9:20:33 PM.
This article is licensed under a Creative Commons Attribution-NonCommercial 3.0 Unported Licence.

organic solvent[11] until new reporting, in 2022, on an F_2PyBTM NHC-Gold(I) complex[12] with 36% photoluminescence quantum yield (PLQY) in dichloromethane and *para*-mesitylated F_2PyBTM (Mes_2F_2PyBTM)[13] with 69% chloroform.

In addition to the idea of substituting the *para*-positions to the radical centre of the PyBTM by two phenyl groups (PyPBTM),[14] *ortho*-methyl groups on the phenyl groups play an important role in enhancing fluorescence.[13] One mesityl group works as an electron-donor in mesitylated PyBTM derivatives and composes a donor–acceptor system with a relatively easily reducible radical centre. The *ortho*-methyl groups obstruct π-conjugation between the mesityl and diphenylpyridylmethyl in the D_0 ground state, and suppress the structural relaxation in the D_1 excited state.

Here, we prepared several new Mes_2F_2PyBTM and Mes_2PyBTM analogues with modified hydrocarbon substituents on the terminal phenyl groups. Detailed effects of these substituents on PLQY and photostability were elucidated.

Results and discussion

First, we attempted to synthesize derivatives with bulkier *ortho*-substituents, expecting higher fluorescence efficiency. Instead of 2,4,6-trimethylphenylboronic acid, we used 2,4,6-triisopropylphenylboronic acid and carried out the Suzuki–Miyaura coupling reaction with a micellar catalysis.[14] Despite the bulkiness of the *ortho*-substituents, the reaction proceeded smoothly, thus producing 2,4,6-triisopropylphenylated αH-PyBTM (precursor of PyBTM) and αH-F_2PyBTM (precursor of F_2PyBTM). In general, the reaction of αH-PyBTM yields fewer byproducts than that of αH-F_2PyBTM. Thanks to the isopropyl groups, we could isolate αH-TippF_2PyBTM (**3H**), although we could not isolate αH-MesF_2PyBTM in our previous report. After deprotonation and oxidation, stable luminescent radicals, TippPyBTM (**1**), Tipp$_2$PyBTM (**2**), TippF_2PyBTM (**3**), and Tipp$_2F_2$PyBTM (**4**) were obtained (Scheme 2 and Fig. S1 for ESR spectra, ESI†).

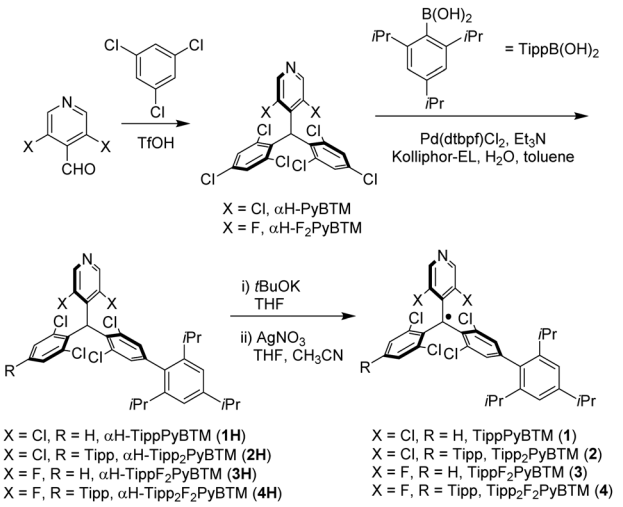

Scheme 2 Synthesis of **1–4**.

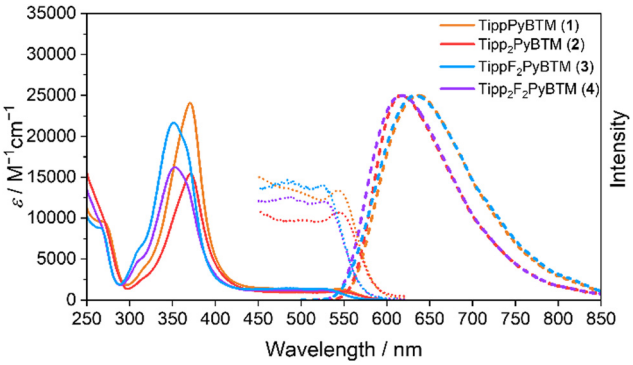

Fig. 1 Absorption (solid line) and emission (broken line, λ_{ex} = 450 nm) spectra of TippPyBTM (**1**, orange), Tipp$_2$PyBTM (**2**, red), TippF_2PyBTM (**3**, light blue), and Tipp$_2F_2$PyBTM (**4**, purple) in dichloromethane. Enlarged portions of the absorption spectra (10 fold) are shown from λ = 450 to 620 nm (dotted lines).

Absorption and emission spectra in dichloromethane of **1**, **2**, and **4** were very similar to their corresponding mesityl radicals (Fig. 1).[13] The lowest energy absorption changes little from PyBTM and F_2PyBTM because the triisopropylphenyl groups are poorly conjugated with the radical moieties at the ground state. In order to estimate structures using DFT, we adopted the UB3LYP level of theory with 6-31G(d, p) basis sets, since they closely reproduced the experimental absorption and emission spectra from previous studies. The solvent effect of dichloromethane was considered by using a polarizable continuum model (PCM).[15] In the DFT optimized structure of **1**, **2**, and **4**, the triisopropylphenyl groups are nearly perpendicular to the bonded dichorophenyl group, similarly to Mes_2F_2PyBTM (Table 1, Table S1 (ESI†), Scheme 3, ϕ_4 and ϕ_5).

On the other hand, the emission maxima of radicals were to some extent redshifted from PyBTM and F_2PyBTM because one of the triisopropylphenyl groups is conjugated by a certain amount with the bonded dichorophenyl group. The TD-DFT optimized dihedral angles between the triisopropylphenyl ring and dichlorophenyl ring (ϕ_4) were *ca.* 54–55°, whereas the dihedral angles between the mesityl ring and dichlorophenyl ring were *ca.* 49–54°. These changes can be explained by the electronic structures, similarly to the cases of mesityl groups. The lowest excitation of these radicals can generally be

Table 1 Calculated torsion angles of the aryl rings of radicals in dichloromethane. Angles outside of brackets are in the D_0 state optimized using UB3LYP/6-31G(d, p). Angles inside the brackets are in the D_1 state optimized using TD-UB3LYP/6-31G(d,p)

	1	**2**	**3**	**4**
φ_1	48° [36°]	48° [37°]	32° [23°]	32° [23°]
φ_2	49° [52°]	49° [52°]	52° [54°]	52° [53°]
φ_3	49° [47°]	49° [48°]	52° [48°]	52° [49°]
ϕ_4	90° [55°]	88° [55°]	89° [54°]	89° [54°]
ϕ_5		88° [87°]		89° [89°]

φ_1: Torsion angle of pyridyl ring. φ_2 and φ_3: torsion angles of dichlorophenyl rings. ϕ_4 and ϕ_5: dihedral angles between dichlorophenyl groups and 2,4,6-triisopropylphenyl groups.

 © 2023 The Author(s). Published by the Royal Society of Chemistry

Open Access Article. Published on 26 September 2023. Downloaded on 12/4/2025 9:20:33 PM.
This article is licensed under a Creative Commons Attribution-NonCommercial 3.0 Unported Licence.

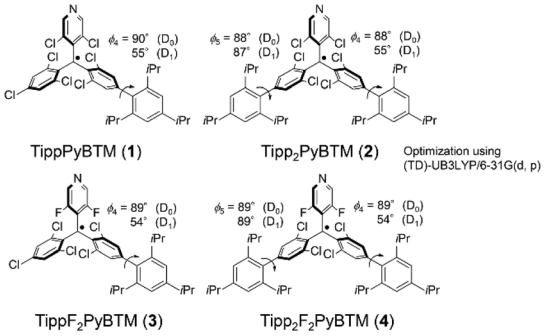

Scheme 3 Dihedral angles between dichlorophenyl groups and 2,4,6-triisopropylphenyl groups.

regarded as the β-spin electron transition from the β-HOMO to the β-LUMO by TD-DFT calculations, where the spin of an unpaired electron of the radical is defined as α-spin. Since the β-HOMOs of **1**, **2**, **3**, and **4** are mainly distributed on one of the triisopropylphenyl groups (Fig. 2), these triisopropylphenyl groups become cationic at the lowest excited state (D_1) by intramolecular electron transfer. The cationic triisopropylphenyl ring seeks conjugation between the bonded dichlorophenyl ring and stabilizes its energy by delocalizing the plus charge.

The PLQYs (Φ_f) of **1**, **2**, and **4** were inferior to those of the corresponding mesityl radicals in both dichloromethane and chloroform (Table 2 and Table S2, ESI†), while **4** in particular was still highly emissive. The PLQYs of the radicals are simply determined by the competition of the rate of fluorescence (k_f) and the rate of the non-radiative decay from the D_1 to D_0.

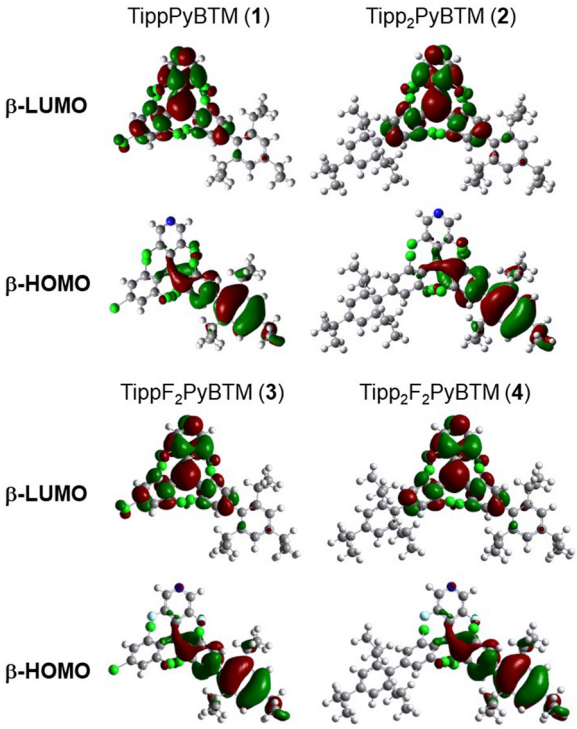

Fig. 2 TD-DFT calculated frontier orbitals of **1**, **2**, **3**, and **4** at the D_1 optimized structure calculated using UB3LYP/6-31G(d,p).

Table 2 PLQYs and photophysical parameters of radicals in dichloromethane

	λ_{em} (nm)	Φ_f (%)	τ/ns	$k_f/10^7$ s^{-1}	$k_{nr}/10^7$ s^{-1}
MesPyBTM	645	30	26	1.2	2.7
1	637	22	22	1.0	3.5
Mes_2PyBTM	628	47	38	1.2	1.4
2	618	39	37	1.1	1.6
3	632	46	32	1.4	1.7
Mes_2F_2PyBTM	623	66	44	1.5	0.8
4	617	62	47	1.3	0.8

Photophysical parameters of MesPyBTM, Mes_2PyBTM, and Mes_2F_2-PyBTM are cited from ref. 13. All Φ_f values were obtained by absolute PLQY measurement.

These parameters can be calculated from measured PLQYs and fluorescence lifetimes. The k_f values of TippPyBTM (**1**), $Tipp_2$-PyBTM (**2**), and $Tipp_2F_2$PyBTM (**4**) were lower than those of MesPyBTM, Mes_2PyBTM, and Mes_2F_2PyBTM, respectively. This effect can be explained by the lower conjugation between the triisopropylphenyl and dichlorophenyl groups, which probably delayed the transition from D_1 to D_0. Actually, the TD-DFT calculated oscillator strengths of the D_0-D_1 transitions at the D_1 optimized structures of **1**, **2**, and **4** were slightly smaller than those of the corresponding mesityl radicals. The k_{nr} values show that the isopropyl groups also do not contribute to decreasing the internal conversion caused by vibronic coupling, and they were rather counterproductive in **1** and **2**.

Previously, it was reported that aryl substitution of PyBTM further improved the photostability of the radicals.[14] However, the photostabilities of MesPyBTM, Mes_2PyBTM, and Mes_2F_2-PyBTM were very near to that of PyBTM. Perpendicular mesityl groups do not help to improve photostability. Similarly, **1**, **2**, **3** and **4** were not more photostable than PyBTM (Fig. S2a and Table S3, ESI†), although they are still much more photostable than TTM.[8] Perpendicular triisopropylphenyl groups also do not help to improve photostability.

In order to clarify the role of *m*-positions on the phenyl groups, we next prepared F_2PyBTM derivatives with 2,3,4,5,6-pentamethylphenyl groups. Ph*F_2PyBTM (**5**) and Ph*$_2F_2$PyBTM (**6**) were synthesized using 2,3,4,5,6-pentamethylphenylboronic acid (Scheme 4). The steric effect of the *ortho*-methyl groups was not expected to change, but the inductive effect of *m*-methyl groups became a matter of interest.

Absorption spectra of these radicals were very similar to that of Mes_2F_2PyBTM (Fig. 3). The pentamethylphenyl group was not conjugated with the radical, similarly to the mesityl and triisopropylphenyl groups. The DFT optimized dihedral angles between the pentamethyl group and the dichlorophenyl group were nearly 90° (Table 3 and Scheme 5). Surprisingly, the fluorescence of **5** and **6** was quite weak (<2%) in dichloromethane. The TD-DFT calculation shows that their first excited state D_1 is almost completely composed of the excitation of the β-spin electron, which is similar to other PyBTM derivatives. The main transition, the β-HOMO–LUMO transition, can be regarded as intramolecular electron transfer from β-HOMO on the added phenyl group to the β-LUMO on the radical moiety.

Open Access Article. Published on 26 September 2023. Downloaded on 12/4/2025 9:20:33 PM.
This article is licensed under a Creative Commons Attribution-NonCommercial 3.0 Unported Licence.

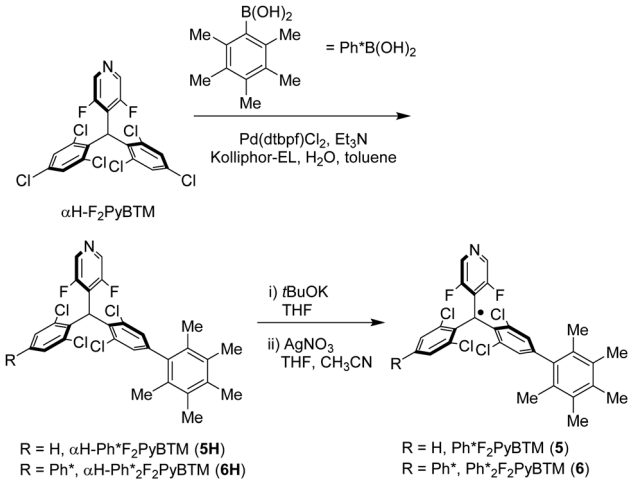

Scheme 4 Synthesis of **5** and **6**.

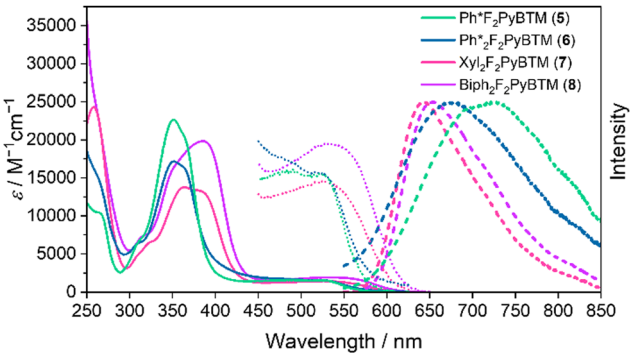

Fig. 3 Absorption (solid line) and emission (broken line, λ_{ex} = 450 nm) spectra of Ph*F_2PyBTM (**5**, pale green), Ph*$_2F_2$PyBTM (**6**, dark green), Xyl$_2$F$_2$PyBTM (**7**, pink), and Biph$_2$F$_2$PyBTM (**8**, pale purple) in dichloromethane. Enlarged portions of the absorption spectra (10 fold) are shown from λ = 450 to 650 nm (dotted lines).

Table 3 Calculated torsion angles of the aryl rings of radicals in dichloromethane. Angles outside of brackets are in the D_0 state optimized using UB3LYP/6-31G(d, p). Angles inside the brackets are in the D_1 state optimized using TD-UB3LYP/6-31G(d,p)

	5	**6**	**7**	**8**
φ_1	32° [25°]	32° [24°]	32° [27°]	32° [25°]
φ_2	52° [50°]	52° [52°]	52° [52°]	52° [50°]
φ_3	53° [51°]	52° [49°]	52° [46°]	52° [48°]
ϕ_4	88° [89°]	88° [88°]	48° [34°]	48° [39°]
ϕ_5		88° [89°]	51° [50°]	50° [49°]
ϕ_6				52° [39°]
ϕ_7				52° [51°]

φ_1: Torsion angle of pyridyl ring. φ_2 and φ_3: torsion angles of dichlorophenyl rings. ϕ_4 and ϕ_5: dihedral angles between dichlorophenyl groups and (alkyl)phenyl groups. ϕ_6 and ϕ_7: dihedral angles between *o*-phenylene groups and phenyl groups.

The β-HOMOs were to some extent delocalized on the dichlorophenyl group in the mesityl and triisopropylphenyl radicals; however, the β-HOMOs of pentamethylphenyl radicals are almost localized on the pentamethyl phenyl groups (Fig. 4), and the dihedral angles between the pentaphenyl and dichlorophenyl groups are still nearly 90° at the D_1 state (Table 3). This means that plus and minus charges at the D_1 state of **5** and **6** are more separated. The luminescence of such radicals tends to be quenched in polar solvents.[11,16]

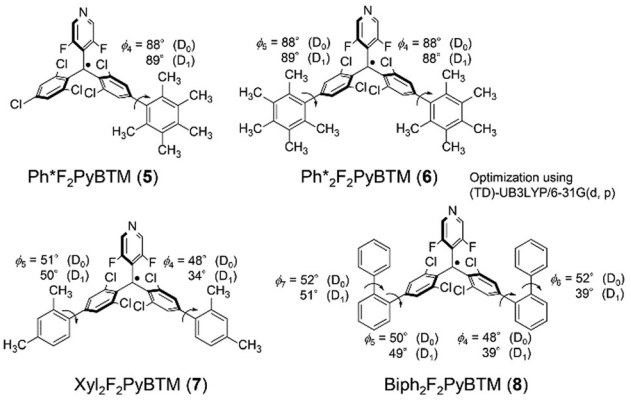

Scheme 5 Dihedral angles between benzene rings.

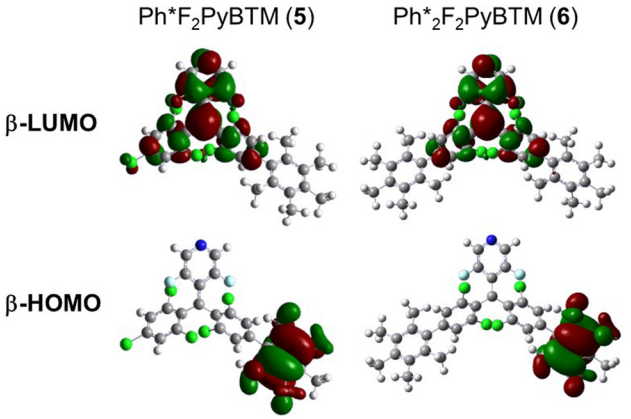

Fig. 4 TD-DFT calculated frontier orbitals of **5** and **6** at the D_1 optimized structure calculated using UB3LYP/6-31G(d,p).

The table of photophysical parameters of Ph*F_2PyBTM (**5**) and Ph*$_2F_2$PyBTM (**6**) show that they have quite large non-radiative decay rates in dichloromethane in addition to small rates of fluorescence. Luminescence quenching in polar organic solvents have been reported in the donor–acceptor system using TTM as an acceptor. Even chloroform (relative permittivity ε_r = 4.8) can largely decrease the PLQY of the carbazole-TTM system.[11ab] In the cases of Ph*F_2PyBTM (**5**) and Ph*$_2F_2$PyBTM (**6**), dichloromethane (ε_r = 9.1) quenches the fluorescence, while chloroform maintains high-efficiency fluorescence (30% and 47%, respectively, Table S2, ESI†). We propose that the minimum polarity of a solvent that can quench the fluorescence is a measure of the degree of polarization at the intramolecular charge transfer excited state in the D–A radical systems.

So far, we have considered PyPBTM derivatives with alkyl groups at double *ortho*-positions. What about the effect of an

 © 2023 The Author(s). Published by the Royal Society of Chemistry

Open Access Article. Published on 26 September 2023. Downloaded on 12/4/2025 9:20:33 PM.
This article is licensed under a Creative Commons Attribution-NonCommercial 3.0 Unported Licence.

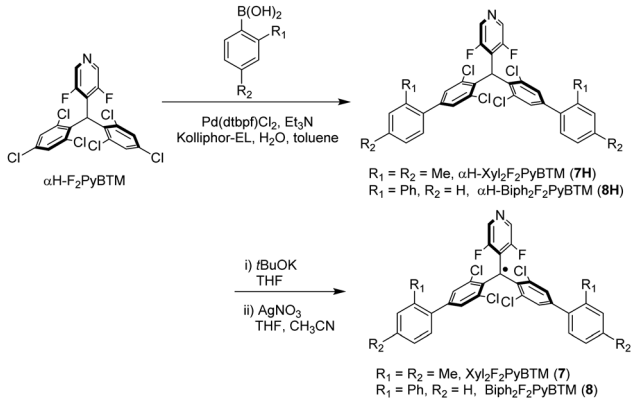

Scheme 6 Synthesis of **7** and **8**.

alkyl group at a single *ortho*-position, and what about the effect of an aryl group at a single *ortho*-position? Using 2,4,-dimethylphenylboronic acid and 2-biphenylboronic acid, we prepared Xyl_2F_2PyBTM (**7**) and $Biph_2F_2PyBTM$ (**8**), respectively (Scheme 6).

Absorption spectra of **7** and **8** show that the lowest energy absorptions of these radicals are slightly redshifted (Fig. 3). This means that the xylyl and biphenyl groups can be conjugated to the radical moieties due to less steric groups at the *ortho*-positions. The DFT-optimized dihedral angles between the dichlorophenyl ring and xylyl or biphenyl were 48–51° at the ground state (Table 3 and Scheme 5). The emission peaks of these radicals were more greatly bathochromically shifted, since the conjugation between dichlorophenyl and xylyl or biphenyl was strengthened. The TD-DFT-optimized dihedral angles were 34° in **7** and 39° in **8** on one side Fig. 5.

Xyl_2F_2PyBTM (**7**) showed bright fluorescence in solutions, and its PLQY was 40% in dichloromethane. The rate of fluorescence (k_f) of **7** was similar to that of Mes_2F_2PyBTM (Tables 2 and 4). The difference in PLQYs between **7** and Mes_2F_2PyBTM derives from the difference in the rate of non-radiative decay (k_{nr}), which is seen in the shorter fluorescence lifetime (26 ns) of **7** compared to the fluorescence lifetime (44 ns) of Mes_2F_2-PyBTM. It was shown that even a single *ortho*-methyl group has

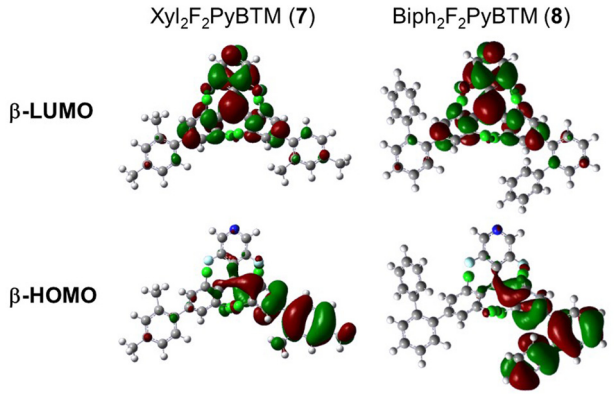

Fig. 5 TD-DFT calculated frontier orbitals of **7** and **8** at the D_1 optimized structure calculated using UB3LYP/6-31G(d,p).

Table 4 PLQYs and photophysical parameters of radicals in dichloromethane

	λ_{em} (nm)	Φ_f (%)	τ/ns	$k_f/10^7$ s^{-1}	$k_{nr}/10^7$ s^{-1}
PyBTM[a]	585	2	6.4	0.3	14
F_2PyBTM[b]	566	4	12.5	0.3	7.7
PyPBTM[c]	654	9.5	12	0.8	7.5
5	725	0.5	0.7	0.7	142
6	670	1.3	2.4	0.5	41
7	642	40	26	1.5	2.3
8	653	15	15	1.0	5.7

[a] Cited from ref. 8. [b] Cited from ref. 9. [c] Cited from ref. 13. All Φ_f values were obtained by absolute PLQY measurement.

a considerable effect in suppressing the non-radiative decay, although it did not reach that of double *ortho*-methyl groups. The PLQY of 15% for **8** was a bit larger than that of PyPBTM, although it showed similar redshifted emission (Table 4). The fluorescence lifetime of **8** was slightly longer than those of F_2PyBTM and PyPBTM, and the rate of fluorescence of **8** was faster than that of PyPBTM.

The photostabilities of Ph*F_2PyBTM (**5**) and Ph*$_2F_2$PyBTM (**6**) in chloroform were clearly improved over that of PyBTM (Fig. S2b and Table S4, ESI†). We speculate that photostability almost entirely depends on the stability of the intramolecular charge transfer excited state. The two additional methyl groups of the pentamethylphenyl group compared to the mesityl group are thought to stabilize the positive charge on the terminal phenyl groups through electronic or steric effects.

Xyl_2F_2PyBTM (**7**) had larger photostability than F_2PyBTM and Mes_2F_2PyBTM in dichloromethane (Fig. 6). The lack of one *ortho*-methyl group can be interpreted as having less protection by methyl groups, but the conjugation between the dichlorophenyl and xylyl groups had a larger stabilization effect. Photostabilization by conjugation between benzene rings is more pronounced in **8**. Conjugation of the phenylene ring with both dichlorophenyl and terminal *ortho*-phenyl rings (Fig. 5) resulted

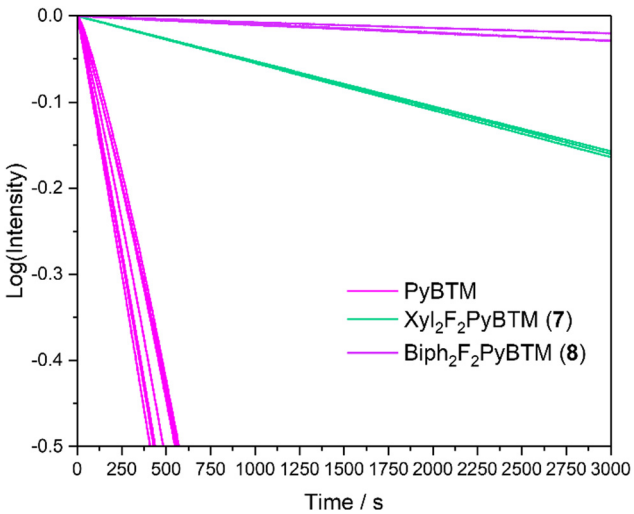

Fig. 6 Plots showing the emission decay of **7** and **8** in dichloromethane under continuous excitation with light at λ_{ex} = 370 nm ± 10 nm.

Open Access Article. Published on 26 September 2023. Downloaded on 12/4/2025 9:20:33 PM.
This article is licensed under a Creative Commons Attribution-NonCommercial 3.0 Unported Licence.

in stabilization of about 100 times that of PyBTM under 370 nm UV irradiation (Table S3, ESI†). These effects are consistent with the previous reports of photostabilization of TTM using carbazole donors and phenyl rings.[17]

Conclusions

We synthesized eight novel photostable radicals and clarified the role of hydrocarbon substituents on the terminal phenyl groups. Isopropy groups at the 2-, (4-,) and 6-positions had the effect of sterically disturbing the conjugation between the dichlorophenyl group and the terminal phenyl group, which had a positive role in the enhancement of fluorescence in the previous case of methyl groups. However, an excessive steric effect was found to slightly detract from the PLQYs. Methyl groups at the 2-, 3-, 4-, 5-, and 6-positions had the effect of strengthening the electron-donor character of the phenyl group. The charge-separated excited state was largely quenched in dichloromethane, whereas a smaller amount of quenching occured in less polar chloroform. Single substitution of the *ortho*-position (2-position) of the terminal phenyl group had certain effects on enhancing the fluorescence compared to no substitution at the *ortho*-position. The effect of the *ortho*-methyl group is indicated to be superior to that of the *ortho*-phenyl group. Compared to the ineffectiveness of the set of 2,4,6-methyl or 2,4,6-triisopropyl groups in the enhancement of photostability, methyl groups at the 3,5-positions or a blank (hydrogen substituent) of the 6-position had a pronounced effect on stabilizing the excited state, thus enhancing the photostability. These findings will be useful in the development of a donor-PyBTM or donor-F_2PyBTM system with high PLQY, high photostability, and other useful functions.

Experimental

Materials and methods

The starting materials, αH-PyBTM and αH-F_2PyBTM was prepared according to the previous report.[8,9] Commercially available compounds were used as received without further purification. The emulsion of toluene in aqueous 2 wt% Kolliphor EL (K-EL) was prepared by mixing a 2 wt% aqueous dispersion of K-EL (1.8 g of K-EL in 88.2 mL of deionized water) with 10 mL of toluene until a stable, milky dispersion was obtained. The emulsion and triethylamine were deoxygenated bubbling argon before use. Preparative recycling gel permeation chromatography was performed with a recycling preparative HPLC, LaboACE LC-5060, Japan Analytical Industry Co., Ltd. ^{1}H (400 MHz) and ^{13}C NMR (100 MHz) spectra were recorded on a JEOL JNM-ECS 400 spectrometer using $CDCl_3$. The residual solvent signals (^{1}H NMR: δ 7.26, ^{13}C NMR: δ 77.16) were used as the internal standards. Gaussian 16 software was used for the DFT and TD-DFT calculations. ESR spectra were recorded with a JEOL JES-FR30EX spectrometer with X-band microwave. Sample solutions were charged in a 2.5 mmϕ sample tube. Magnetic field was calibrated with the Mn^{2+}/MgO standard. Mass spectrometry was performed with a JEOL-JMS-S3000 (MALDI-Spiral-TOF MS) mass spectrometer with DCTB (20 mg/mL in $CHCl_3$) as a matrix and TFANa (1 mg mL^{-1} in THF) as a cationization agent. Absorption and emission spectra were monitored on Hitachi U-4150 spectrophotometer and Hitachi F-7100 fluorescence spectrophotometer, respectively. Photostability under 370 nm light were recorded with a JASCO FP-8600KS spectrofluorometer. Absolute luminescence quantum yields were measured using Hamamatsu Photonics Quantaurus QY. Photoluminescence decay curves were measured using a measurement system with a picosecond diode laser with the emission wavelength of 375 nm (Advanced Laser Diode Systems PIL037X) as light source, a single grating spectrometer (Andor Kymera193i-B1), and a photon counting detector (MPD SPD-050-CTE) operated with a time-correlated single photon counting (TCSPC) technique. Elemental analysis was conducted at NAIST (**1**, **2**, **3**, **5**, **8**) and Center for Organic Elemental Microanalysis, Graduate School of Pharmaceutical Sciences, Kyoto University (**4**, **6**, **7**).

Synthesis of αH-TippPyBTM (1H) and αH-Tipp$_2$PyBTM (2H)

In a Schlenk tube αH-PyBTM (521 mg, 1.00 mmol), 2,4,6-triisopropylphenylboronic acid (744 mg, 3.00 mmol), Pd(dtbpf)Cl_2 (65.2 mg, 0.100 mmol), were put under an argon atmosphere. Degassed K-EL 2 wt%: water : toluene (9 : 1 v/v) emulsion (3.5 mL) was added, and the mixture was heated at 70 °C. Degassed triethylamine (1.2 mL, 8.6 mmol) was finally added, and the reaction mixture was stirred at 70 °C overnight. The reaction mixture was cooled down to room temperature, added chloroform, and filtered on a pad of silica and sodium sulfate. The solvent was evaporated and purified by silica gel column chromatography ($CHCl_3$: hexane = 1 : 1). The yellow oil (806 mg) was separated by GPC ($CHCl_3$) to obtain pure **1H** (240 mg, 0.348 mmol, 35%) and **2H** (113 mg, 0.132 mmol, 13%).

1H (1 : 1 mixture of two conformers). ^{1}H NMR (400 MHz, $CDCl_3$, ppm): δ 8.52 (s, 0.5H), 8.50 (s, 0.5H), 8.39 (s, 0.5H), 8.38 (s, 0.5H), 7.44 (d, J = 2.1 Hz, 0.5H), 7.40 (d, J = 2.2 Hz, 0.5H), 7.31 (d, J = 2.2 Hz, 0.5H), 7.26 (br, 0.5H), 7.22 (d, J = 1.5 Hz, 0.5H), 7.21 (d, J = 1.6 Hz, 0.5H), 7.10 (d, J = 1.5 Hz, 0.5H), 7.07 (d, J = 1.6 Hz, 0.5H), 7.05 (s, 2H), 6.83 (s, 0.5H), 6.83 (s, 0.5H), 2.93 (sep, J = 6.9 Hz, 1H), 2.66–2.54 (m, 2H), 1.29 (d, J = 6.9, Hz, 6H), 1.15–1.04 (m, 12H).

^{13}C NMR (100 MHz, $CDCl_3$, ppm): δ 149.7, 149.5, 149.1, 147.9, 147.8, 146.3, 146.2, 144.2, 144.1, 142.9, 142.8, 138.1, 138.0, 137.4, 137.4, 137.0, 137.0, 136.4, 134.6, 134.5, 134.2, 134.1, 133.9, 133.7, 133.7, 133.6, 133.3, 132.1, 131.9, 131.8, 131.6, 130.5, 130.1, 130.0, 129.9, 128.8, 128.5, 120.9, 120.8, 50.0, 34.5, 30.6, 30.5, 24.3, 24.3, 24.2, 24.0.

HRMS (MALDI-TOF MS positive mode) m/z: $[MH]^+$ calcd for $C_{33}H_{31}Cl_7N^+$ 686.02707; found 686.02764.

2H. ^{1}H NMR (400 MHz, $CDCl_3$, ppm): δ 8.53 (s, 1H), 8.40 (s, 1H), 7.27 (d, J = 1.7 Hz, 1H), 7.23 (d, J = 1.7 Hz, 1H), 7.13 (d, J = 1.7 Hz, 1H), 7.08 (d, J = 1.7 Hz, 1H), 7.06 (br, 4H), 6.95 (s, 1H), 2.94 (sep, J = 6.9 Hz, 2H), 2.72–2.57 (m, 4H), 1.30 (dd, J = 6.9, 1.4 Hz, 12H), 1.16–1.07 (m, 24H).

^{13}C NMR (100 MHz, $CDCl_3$, ppm): δ 149.6, 149.1, 147.9, 146.5, 146.3, 146.3, 144.9, 142.6, 137.1, 137.0, 136.7, 136.3, 134.7, 134.1, 134.0, 133.9, 132.8, 132.2, 132.0, 131.7, 130.0,

 © 2023 The Author(s). Published by the Royal Society of Chemistry

Open Access Article. Published on 26 September 2023. Downloaded on 12/4/2025 9:20:33 PM.
This article is licensed under a Creative Commons Attribution-NonCommercial 3.0 Unported Licence.

130.0, 120.9, 50.3, 30.6, 30.6, 30.5, 30.4, 24.5, 24.3, 24.3, 24.3, 24.3, 24.1, 24.1.

HRMS (MALDI-TOF MS positive mode) *m*/*z*: $[MH]^+$ calcd for $C_{48}H_{54}Cl_6N^+$ 854.23819; found 854.23855.

Synthesis of αH-TippF$_2$PyBTM (3H) and αH-Tipp$_2$F$_2$PyBTM (4H)

In a Schlenk tube αH-F$_2$PyBTM (489 mg, 1.00 mmol), 2,4,6-tri-isopropylphenylboronic acid (746 mg, 3.01 mmol), Pd(dtbpf)Cl$_2$ (52.3 mg, 0.0802 mmol), were put under an argon atmosphere. Degassed K-EL 2 wt%: water : toluene (9 : 1 v/v) emulsion (3.5 mL) was added, and the mixture was heated at 80 °C. Degassed triethylamine (0.85 mL, 6.1 mmol) was finally added, and the reaction mixture was stirred at 80 °C overnight. The reaction mixture was cooled down to room temperature, added dichloromethane, and filtered on a Celite pad. The solvent was evaporated and purified by silica gel column chromatography (CHCl$_3$: hexane = 1 : 1). The mixture was separated by GPC (CHCl$_3$) to obtain crude **3H** (291 mg, 44%) and pure **4H** (128 mg, 0.195 mmol, 20%). Recrystallization of crude **3H** from dichloromethane-methanol twice gave pure **3H** (69.8 mg, 0.106 mmol, 11%).

3H. ^{1}H NMR (400 MHz, CDCl$_3$, ppm): δ 8.36 (s, 1H), 8.24 (s, 1H), 7.36 (s, 2H), 7.15 (s, 2H), 7.04 (s, 2H), 6.76 (s, 1H), 2.92 (sep, J = 6.9 Hz, 1H), 2.57 (sep, J = 6.8 Hz, 4H), 1.28 (d, J = 6.9 Hz, 6H), 1.11 (d, J = 6.8 Hz, 6H), 1.10 (d, J = 6.8 Hz, 6H).

^{13}C NMR (100 MHz, CDCl$_3$, ppm): δ 149.1, 146.3, 142.8, 137.2, 136.1, 135.4, 134.2, 133.8, 133.0, 131.4, 131.0, 129.6, 120.8, 42.0, 34.5, 30.5, 24.3, 24.2, 24.1.

HRMS(MALDI-TOF MS positive mode) *m*/*z*: $[MH]^+$ calcd for $C_{33}H_{31}Cl_5NF_2^+$ 654.08617; found 654.08662.

4H. ^{1}H NMR (400 MHz, CDCl$_3$, ppm): δ 8.38 (s, 1H), 8.25 (s, 1H), 7.17 (s, 4H), 7.05 (s, 4H), 6.88 (s, 1H), 2.93 (sep, J = 6.9 Hz, 2H), 2.62 (sep, J = 6.8 Hz, 4H), 1.30 (d, J = 6.9 Hz, 12H), 1.13 (d, J = 6.8 Hz, 12H), 1.12 (d, J = 6.8 Hz, 12H).

^{13}C NMR (100 MHz, CDCl$_3$, ppm): δ 149.1, 146.4, 142.5, 136.1, 135.3, 135.1, 134.0, 133.8, 133.6, 132.1, 131.0, 125.5, 125.4, 125.2, 120.9, 42.4, 42.3, 34.5, 30.5, 24.4, 24.3, 24.2.

HRMS (MALDI-TOF MS positive mode) *m*/*z*: $[MH]^+$ calcd for $C_{48}H_{54}Cl_4NF_2^+$ 822.29729; found 822.29764.

Synthesis of αH-Ph*PyBTM (5H) and αH-Ph*$_2$F$_2$PyBTM (6H)

In a Schlenk tube αH-F$_2$PyBTM (330 mg, 0.675 mmol), 2,3,4,5,6-pentamethylphenylboronic acid (414 mg, 2.16 mmol), Pd(dtbpf)Cl$_2$ (43 mg, 0.066 mmol), were put under an argon atmosphere. Degassed K-EL 2 wt%: water : toluene (9 : 1 v/v) emulsion (2.4 mL) was added, and the mixture was heated at 70 °C. Degassed triethylamine (0.56 mL, 4.0 mmol) was finally added, and the reaction mixture was stirred at 70 °C overnight. The reaction mixture was cooled down to room temperature, added chloroform, and filtered on a Celite pad. The solvent was evaporated and purified by silica gel column chromatography (CHCl$_3$: hexane = 1 : 1). The mixture (538 mg) was separated by GPC (CHCl$_3$) to obtain crude **5H** (224 mg, 55%) and **6H** (91 mg, 19%). Recrystallization from dichloromethane-methanol gave **5H** (142 mg, 24%) and **6H** (35 mg, 0.049 mmol, 7.3%).

5H. ^{1}H NMR (400 MHz, CDCl$_3$, ppm): δ 8.35 (s, 1H), 8.23 (s, 1H), 7.35 (s, 2H), 7.08 (s, 2H), 6.74 (s, 1H), 2.29 (s, 3H), 2.24 (s, 6H), 1.95 (s, 6H).

^{13}C NMR (100 MHz, CDCl$_3$, ppm): δ 145.0, 137.2, 136.6, 136.5, 135.4, 135.1, 134.1, 133.6, 132.8, 131.3, 131.3, 130.8, 129.5, 124.8, 124.7, 124.6, 42.1, 42.0, 18.5, 17.0, 16.7.

HRMS (MALDI-TOF MS positive mode) *m*/*z*: $[MH]^+$ calcd for $C_{29}H_{23}Cl_5NF_2^+$ 598.02357; found 598.02323.

6H. ^{1}H NMR (400 MHz, CDCl$_3$, ppm): δ 8.37 (s, 1H), 8.25 (s, 1H), 7.10 (s, 4H), 6.86 (s, 1H), 2.29 (s, 6H), 2.25 (s, 12H), 1.97 (s, 12H).

^{13}C NMR (100 MHz, CDCl$_3$, ppm): δ 144.7, 136.7, 136.5, 135.4, 135.3, 135.1, 133.7, 133.5, 132.8, 132.0, 131.4, 131.0, 130.7, 125.2, 42.3, 18.6, 17.0, 16.7.

HRMS(MALDI-TOF MS positive mode) *m*/*z*: $[MH]^+$ calcd for $C_{40}H_{38}Cl_4NF_2^+$ 710.17209; found 710.17249.

Synthesis of αH-Xyl$_2$F$_2$PyBTM (7H)

In a Schlenk tube αH-F$_2$PyBTM (244 mg, 0.500 mmol), 2,4-dimethylphenylboronic acid (225 mg, 1.50 mmol), Pd(dtbpf)Cl$_2$ (32.6 mg, 0.0500 mmol), were put under an argon atmosphere. Degassed K-EL 2 wt%: water : toluene (9 : 1 v/v) emulsion (1.8 mL) was added, and the mixture was heated at 70 °C. Degassed triethylamine (0.45 mL, 3.2 mmol) was finally added, and the reaction mixture was stirred at 70 °C overnight. The reaction mixture was cooled down to room temperature, added chloroform, and filtered on a Celite pad. The solvent was evaporated and purified by silica gel column chromatography (CHCl$_3$: hexane = 1 : 1). The mixture was separated by GPC (CHCl$_3$) to obtain crude **7H** and monoadduct. (58 mg, *ca.* 20%). Recrystallization from dichloromethane-methanol gave **7H** (25.0 mg, 0.040 mmol, 8.0%).

^{1}H NMR (400 MHz, CDCl$_3$, ppm): δ 8.36 (s, 1H), 8.24 (s, 1H), 7.27 (s, 4H), 7.12 (d, 2H. J = 7.8 Hz), 7.09 (s, 2H), 7.06 (d, 2H. J = 7.8 Hz), 6.84 (s, 1H), 2.36 (s, 6H), 2.26 (s, 6H).

^{13}C NMR (100 MHz, CDCl$_3$, ppm): δ 143.4, 138.2, 136.2, 135.8, 135.1, 132.1, 131.5, 130.3, 129.5, 126.9, 42.2, 21.2, 20.4.

HRMS (MALDI-TOF MS positive mode) *m*/*z*: $[MH]^+$ calcd for $C_{34}H_{26}Cl_4NF_2^+$ 626.07819; found 626.07819.

Synthesis of αH-Biph$_2$F$_2$PyBTM (8H)

In a Schlenk tube αH-F$_2$PyBTM (245 mg, 0.502 mmol), 2-biphenylboronic acid (396 mg, 2.00 mmol), Pd(dtbpf)Cl$_2$ (33 mg, 0.051 mmol), were put under an argon atmosphere. Degassed K-EL 2 wt%: water : toluene (9 : 1 v/v) emulsion (1.8 mL) was added, and the mixture was heated at 70 °C. Degassed triethylamine (0.42 mL, 3.0 mmol) was finally added, and the reaction mixture was stirred at 70 °C overnight. The reaction mixture was cooled down to room temperature, added chloroform, and filtered on a Celite pad. The solvent was evaporated and purified by silica gel column chromatography (CHCl$_3$: hexane = 1 : 1). The mixture was separated by GPC (CHCl$_3$) to obtain crude **8H** (195 mg, *ca.* 54%). Recrystallization from dichloromethane-methanol three times gave pure **8H** (177 mg, 0.245 mmol, 49%).

Open Access Article. Published on 26 September 2023. Downloaded on 12/4/2025 9:20:33 PM.
This article is licensed under a Creative Commons Attribution-NonCommercial 3.0 Unported Licence.

^{1}H NMR (400 MHz, $CDCl_3$, ppm): δ 8.30 (s, 1H), 8.19 (s, 1H), 7.46–7.43 (m, 8H), 7.25–7.23 (m, 6H), 7.12–7.10 (m, 4H), 7.04 (s, 4H), 6.63 (s, 1H).

^{13}C NMR (100 MHz, $CDCl_3$, ppm): δ 142.9, 140.9, 140.4, 137.4, 136.0, 135.2, 134.9, 133.6, 133.4, 131.8, 130.8, 130.7, 130.0, 128.7, 128.2, 127.8, 127.2, 125.0, 42.0.

HRMS (MALDI-TOF MS positive mode) *m*/*z*: $[MH]^+$ calcd for $C_{42}H_{26}Cl_4NF_2^+$ 722.07819; found 722.07761.

Synthesis of TippPyBTM (1)

Under an argon atmosphere, αH-TippPyBTM (**1H**, 108.1 mg, 0.157 mmol) was dissolved in dry THF (~3 mL), and *t*BuOK in THF (1 M solution, 0.3 mL, 1.9 eq.) was added. The reaction mixture was stirred overnight in the dark. Silver nitrate (87.5 mg, 0.515 mmol) in acetonitrile (1.6 mL) was added and stirred for 2.5 h. The reaction mixture was added chloroform, filtered on a Celite pad, evaporated and purified by flash chromatography on silica gel ($CHCl_3$: hexane = 1 : 1) and dried *in vacuo* to afford **1** (96.6 mg, 0.140 mmol, 89%) as a red solid.

Elemental analysis calcd for $C_{33}H_{29}Cl_7N$: C 57.63, H 4.25, N 2.04, found: C 57.98, H 4.18, N 2.11.

HRMS (MALDI-TOF MS negative mode) *m*/*z*: $[M]^-$ calcd for $C_{33}H_{29}Cl_7N^-$ 684.01142; found 684.01141.

Synthesis of Tipp$_2$PyBTM (2)

Under an argon atmosphere, αH-Tipp$_2$PyBTM (**2H**, 60.0 mg, 0.0700 mmol) was dissolved in dry THF (3 mL), and *t*BuOK in THF (1 M solution, 0.15 mL, 2.1 eq.) was added. The reaction mixture was stirred overnight in the dark. Silver nitrate (40.2 mg, 0.237 mmol) in acetonitrile (~0.7 mL) was added and stirred for 2.25 h. The reaction mixture was filtered on a Celite pad, and the solvent was evaporated. The crude product was purified by silica gel column chromatography ($CHCl_3$: hexane = 1 : 1) and dried *in vacuo* to afford **2** (53.7 mg, 0.0628 mmol, 90%) as a red solid.

Elemental analysis calcd for $C_{48}H_{52}Cl_6N$: C 67.38, H 6.13, N 1.64, found: C 67.61, H 6.12, N 1.51.

HRMS (MALDI-TOF MS negative mode) *m*/*z*: $[M]^-$ calcd for $C_{48}H_{52}Cl_6N^-$ 852.22364; found 852.22402.

Synthesis of TippF$_2$PyBTM (3)

Under an argon atmosphere, αH-TippPyBTM (**3H**, 44 mg, 0.067 mmol) was dissolved in dry THF (2 mL), and *t*BuOK in THF (1 M solution, 0.10 mL, 1.5 eq.) was added. The reaction mixture was stirred overnight in the dark. Silver nitrate (29.9 mg, 0.176 mmol) in acetonitrile (0.6 mL) was added and stirred for 2.2 h. The reaction mixture was filtered on a Celite pad, and the solvent was evaporated. The crude product was purified by silica gel column chromatography ($CHCl_3$: hexane = 1 : 1) and dried *in vacuo* to afford **3** (44 mg, 0.067 mmol, quant.) as a red solid.

Elemental analysis calcd for $C_{33}H_{29}Cl_5F_2N$: C 60.53, H 4.46, N 2.14, found: C 60.64, H 4.36, N 2.00.

HRMS (MALDI-TOF MS negative mode) *m*/*z*: $[M]^-$ calcd for $C_{33}H_{29}Cl_5NF_2^-$ 652.07162; found 652.07115.

Synthesis of Tipp$_2$F$_2$PyBTM (4)

Under an argon atmosphere, αH-Tipp$_2$F$_2$PyBTM (**4H**, 49.2 mg, 0.0597 mmol) was dissolved in dry THF (3 mL), and *t*BuOK in THF (1 M solution, 0.12 mL, 2.0 eq.) was added. The reaction mixture was stirred overnight in the dark. Silver nitrate (49.6 mg, 0.292 mmol) in acetonitrile (0.8 mL) was added and stirred for 2.25 h. The mixture was added chloroform and filtered on a Celite pad. The solvent was evaporated and the reaction mixture was purified by silica gel column chromatography ($CHCl_3$: hexane = 1 : 2) and dried *in vacuo* to afford **4** (46.0 mg, 0.0559 mmol, 93%) as a red solid.

Elemental analysis calcd for $C_{48}H_{52}Cl_4F_2N$: C 70.07, H 6.37, N 1.70, found: C 70.30, H 6.55, N 1.64.

HRMS (MALDI-TOF MS negative mode) *m*/*z*: $[M]^-$ calcd for $C_{48}H_{52}Cl_4NF_2^-$ 820.28274; found 820.28223.

Synthesis of Ph*F$_2$PyBTM (5)

Under an argon atmosphere, αH-Ph*F$_2$PyBTM (**5H**, 46.2 mg, 0.0770 mmol) was dissolved in dry THF (3 mL), and *t*BuOK in THF (1 M solution, 0.1 mL, 1.3 eq.) was added. The reaction mixture was stirred overnight in the dark. Silver nitrate (40.7 mg, 0.240 mmol) in acetonitrile (0.6 mL) was added and stirred for 2.5 h. The mixture was added chloroform and filtered on a Celite pad. The solvent was evaporated and the reaction mixture was purified by silica gel column chromatography ($CHCl_3$: hexane = 1 : 1) and dried *in vacuo* to afford **5** (38.8 mg, 0.0648 mmol, 84%) as a red solid.

Elemental analysis calcd for $C_{29}H_{21}Cl_5F_2N$: C 58.18, H 3.54, N 2.34, found: C 58.03, H 3.25, N 2.30.

HRMS (MALDI-TOF MS negative mode) *m*/*z*: $[M]^-$ calcd for $C_{29}H_{21}Cl_5NF_2^-$ 596.00902; found 596.00916.

Synthesis of Ph*$_2$F$_2$PyBTM (6)

Under an argon atmosphere, αH-Ph*$_2$F$_2$PyBTM (**6H**, 24.3 mg, 0.0342 mmol) was dissolved in dry THF (3 mL), and *t*BuOK in THF (1 M solution, 0.1 mL, 2.9 eq.) was added. The reaction mixture was stirred overnight in the dark. Silver nitrate (34.8 mg, 0.205 mmol) in acetonitrile (0.5 mL) was added and stirred for 2.5 h. The mixture was added chloroform and filtered on a Celite pad. The solvent was evaporated and the reaction mixture was purified by silica gel column chromatography ($CHCl_3$: hexane = 1 : 1) and dried *in vacuo* to afford **4** (20.5 mg, 0.0289 mmol, 84%) as a red solid.

Elemental analysis calcd for $C_{40}H_{36}Cl_4F_2N$: C 67.62, H 5.11, N 1.97, found: C 67.25, H 5.25, N 2.00.

HRMS (MALDI-TOF MS negative mode) *m*/*z*: $[M]^-$ calcd for $C_{40}H_{36}Cl_4NF_2^-$ 708.15754; found 708.15708.

Synthesis of Xyl$_2$F$_2$PyBTM (7)

Under an argon atmosphere, αH-Xyl$_2$F$_2$PyBTM (**7H**, 20.9 mg, 0.0333 mmol) was dissolved in dry THF (3 mL), and *t*BuOK in THF (1 M solution, 0.1 mL, 3.0 eq.) was added. The reaction mixture was stirred overnight in the dark. Silver nitrate (39.9 mg, 0.234 mmol) in acetonitrile (0.6 mL) was added and stirred for 2.5 h. The mixture was added chloroform and

 © 2023 The Author(s). Published by the Royal Society of Chemistry

Open Access Article. Published on 26 September 2023. Downloaded on 12/4/2025 9:20:33 PM. This article is licensed under a Creative Commons Attribution-NonCommercial 3.0 Unported Licence.

filtered on a Celite pad. The solvent was evaporated and the reaction mixture was purified by silica gel column chromatography ($CHCl_3$: hexane = 1 : 1) and dried *in vacuo* to afford **5** (20 mg, 0.032 mmol, 96%) as a red solid.

Elemental analysis calcd for $C_{34}H_{24}Cl_4F_2N$ + 0.2$CHCl_3$: C 63.17, H 3.75, N 2.15, found: C 63.03, H 3.86, N 2.13.

HRMS (MALDI-TOF MS negative mode) *m*/*z*: $[M]^-$ calcd for $C_{34}H_{24}Cl_4NF_2^-$ 624.06364; found 624.06312.

Synthesis of $Biph_2F_2PyBTM$ (8)

Under an argon atmosphere, αH-$BiPh_2F_2PyBTM$ (**8H**, 72.4 mg, 0.100 mmol) was dissolved in dry THF (3 mL), and *t*BuOK in THF (1 M solution, 0.2 mL, 2.0 eq.) was added. The reaction mixture was stirred overnight in the dark. Silver nitrate (61.8 mg, 0.364 mmol) in acetonitrile (0.9 mL) was added and stirred for 2.5 h. The mixture was added chloroform and filtered on a Celite pad. The solvent was evaporated and the reaction mixture was purified by silica gel column chromatography ($CHCl_3$: hexane = 1 : 1) and dried *in vacuo* to afford **6** (69.6 mg, 0.0963 mmol, 96%) as a red solid.

Elemental analysis calcd for $C_{42}H_{24}Cl_4F_2N$: C 69.83, H 3.35, N 1.94, found: C 69.71, H 3.30, N 1.81.

HRMS (MALDI-TOF MS negative mode) *m*/*z*: $[M]^-$ calcd for $C_{42}H_{24}Cl_4NF_2^-$ 720.06364; found 720.06349.

Author contributions

Y. H. conceived the project. Y. H., R. K., A. B. and K. Y. prepared the compounds. Y. H. conducted the DFT calculations. Y. H. and R. M. did the photophysical measurements. Y. H. wrote original draft, and R. M., T. K., and K. U. reviewed and edited.

Conflicts of interest

There are no conflicts to declare.

Acknowledgements

We thank Prof. Takehiro Kawauchi, Ryukoku University for absolute luminescence quantum yield measurements. We acknowledge support by Ms Yoshiko Nishikawa and Ms Mieko Yamagaki for HRMS (MALDI-TOF MS) and Mr Fumio Asanoma for elemental analysis conducted in NAIST. This work was partly supported by the ARIM Program of the Ministry of Education, Culture, Sports, Science and Technology (MEXT), Japan (JPMXP1222NR0016, JPMXP1223NR0017 and JPMXP1222MS0011). This research was supported by 2022 Ryukoku University Science and Technology Fund, JSPS KAKENHI Grant Number JP20H02759 in Scientific Research (B), JP20K15304 in Early-Career-Scientists and Japan Science and Technology Agency, CREST program Grant Number JPMJCR17N2.

Notes and references

1 (*a*) Q. Peng, A. Obolda, M. Zhang and F. Li, Organic Light-Emitting Diodes Using a Neutral π Radical as Emitter: The Emission from a Doublet, *Angew. Chem., Int. Ed.*, 2015, **54**, 7091–7095; (*b*) X. Ai, E. W. Evans, S. Dong, A. J. Gillett, H. Guo, Y. Chen, T. J. H. Hele, R. H. Friend and F. Li, Efficient radical-based light-emitting diodes with doublet emission, *Nature*, 2018, **563**, 536–540; (*c*) H. Guo, Q. Peng, X.-K. Chen, Q. Gu, S. Dong, E. W. Evans, A. J. Gillett, X. Ai, M. Zhang, D. Credgington, V. Coropceanu, R. H. Friend, J.-L. Brédas and F. Li, High stability and luminescence efficiency in donor–acceptor neutral radicals not following the Aufbau principle, *Nat. Mater.*, 2019, **18**, 977–984; (*d*) A. Abdurahman, T. J. H. Hele, Q. Gu, J. Zhang, Q. Peng, M. Zhang, R. H. Friend, F. Li and E. W. Evans, Understanding the luminescent nature of organic radicals for efficient doublet emitters and pure-red light-emitting diodes, *Nat. Mater.*, 2020, **19**, 1224–1229; (*e*) F. Li, A. J. Gillett, Q. Gu, J. Ding, Z. Chen, T. J. H. Hele, W. K. Myers, R. H. Friend and E. W. Evans, Singlet and triplet to doublet energy transfer: improving organic light-emitting diodes with radicals, *Nat. Commun.*, 2022, **13**, 2744.

2 (*a*) A. Ghirri, C. Bonizzoni, F. Troiani, N. Buccheri, L. Beverina, A. Cassinese and M. Affronte, Coherently coupling distinct spin ensembles through a high-T_c superconducting resonator, *Phys. Rev. A*, 2016, **93**, 063855; (*b*) Y. Hattori, S. Kimura, T. Kusamoto, H. Maeda and H. Nishihara, Cation-responsive turn-on fluorescence and absence of heavy atom effects of pyridyl-substituted triarylmethyl radicals, *Chem. Commun.*, 2018, **54**, 615–618; (*c*) C.-H. Liu, E. Hamzehpoor, Y. Sakai-Otsuka, T. Jadhav and D. F. Perepichka, A Pure-Red Doublet Emission with 90% Quantum Yield: Stable, Colorless, Iodinated Triphenylmethane Solid, *Angew. Chem., Int. Ed.*, 2020, **59**, 23030–23034; (*d*) Z. Zhou, C. Qiao, J. Yao, Y. Yan and Y. S. Zhao, Exciton funneling amplified photoluminescence anisotropy in organic radical-doped microcrystals, *J. Mater. Chem. C*, 2022, **10**, 2551–2555.

3 (*a*) S. Kimura, T. Kusamoto, S. Kimura, K. Kato, Y. Teki and H. Nishihara, Magnetoluminescence in a Photostable, Brightly Luminescent Organic Radical in a Rigid Environment, *Angew. Chem., Int. Ed.*, 2018, **57**, 12711–12715; (*b*) K. Kato, S. Kimura, T. Kusamoto, H. Nishihara and Y. Teki, Luminescent Radical-Excimer: Excited-State Dynamics of Luminescent Radicals in Doped Host Crystals, *Angew. Chem., Int. Ed.*, 2019, **58**, 2606–2611; (*c*) S. Kimura, S. Kimura, K. Kato, Y. Teki, H. Nishihara and T. Kusamoto, A ground-state-dominated magnetic field effect on the luminescence of stable organic radicals, *Chem. Sci.*, 2021, **12**, 2025–2029; (*d*) S. Kimura, R. Matsuoka, S. Kimura, H. Nishihara and T. Kusamoto, Radical-Based Coordination Polymers as a Platform for Magnetoluminescence, *J. Am. Chem. Soc.*, 2021, **143**, 5610–5615; (*e*) R. Matsuoka, S. Kimura, T. Miura, T. Ikoma and T. Kusamoto, Single-Molecule Magnetoluminescence from a Spatially Confined

Open Access Article. Published on 26 September 2023. Downloaded on 12/4/2025 9:20:33 PM.
This article is licensed under a Creative Commons Attribution-NonCommercial 3.0 Unported Licence.

Persistent Diradical Emitter, *J. Am. Chem. Soc.*, 2023, **145**, 13615–13622.

4 (*a*) Y. Beldjoudi, M. A. Nascimento, Y. J. Cho, H. Yu, H. Aziz, D. Tonouchi, K. Eguchi, M. M. Matsushita, K. Awaga, I. Osorio-Roman, C. P. Constantinides and J. M. Rawson, Multifunctional Dithiadiazolyl Radicals: Fluorescence, Electroluminescence, and Photoconducting Behavior in Pyren-1′-yl-dithiadiazolyl, *J. Am. Chem. Soc.*, 2018, **140**, 6260–6270; (*b*) M. Ito, S. Shirai, Y. Xie, T. Kushida, N. Ando, H. Soutome, K. J. Fujimoto, T. Yanai, K. Tabata, Y. Miyata, H. Kita and S. Yamaguchi, Fluorescent Organic π-Radicals Stabilized with Boron: Featuring a SOMO–LUMO Electronic Transition, *Angew. Chem., Int. Ed.*, 2022, e202201965; (*c*) X. Li, Y.-L. Wang, C. Chem, Y.-Y. Ren and Y.-F. Han, A platform for blue-luminescent carbon-centered radicals, *Nat. Commun.*, 2022, **13**, 5367.

5 (*a*) P. Murto and H. Bronstein, Electro-optical π-radicals: design advances, applications and future perspectives, *J. Mater. Chem. C*, 2022, **10**, 7368–7403; (*b*) R. Matsuoka, A. Mizuno, T. Mibu and T. Kusamoto, Luminescence of doublet molecular systems, *Coord. Chem. Rev.*, 2022, **467**, 214646.

6 O. Armet, J. Veciana, C. Rovira, J. Riera, J. Casteñer, E. Molins, J. Rius, C. Miravitlles, S. Olivella and J. Brichfeus, Inert carbon free radicals. 8. Polychlorotriphenylmethyl radicals: synthesis, structure, and spin-density distribution, *J. Phys. Chem.*, 1987, **91**, 5608–5616.

7 M. Ballester and G. de la Fuente, Synthesis and isolation of a perchlorotriphenylcarbanion salt, *Tetrahedron Lett.*, 1970, **11**, 4509–4510.

8 Y. Hattori, T. Kusamoto and H. Nishihara, Luminescence, Stability, and Proton Response of an Open-Shell (3,5-Dichloro-4-pyridyl)bis(2,4,6-trichlorophenyl)methyl Radical, *Angew. Chem., Int. Ed.*, 2014, **53**, 11845–11848.

9 Y. Hattori, T. Kusamoto and H. Nishihara, Highly photostable luminescent open-shell (3,5-dihalo-4-pyridyl)bis-(2,4,6-trichlorophenyl)methyl radicals: significant effects of halogen atoms on their photophysical and photochemical properties, *RSC Adv.*, 2015, **5**, 64802–64805.

10 (*a*) Y. Hattori, T. Kusamoto and H. Nishihara, Enhanced Luminescent Properties of an Open-Shell (3,5-Dichloro-4-pyridyl)bis(2,4,6-trichlorophenyl)methyl Radical by Coordination to Gold, *Angew. Chem., Int. Ed.*, 2015, **54**, 3731–3734; (*b*) T. Kusamoto, Y. Hattori, A. Tanushi and H. Nishihara, Intramolecular Ferromagnetic Radical–Cu^{II} Coupling in a Cu^{II} Complex Ligated with Pyridyl-Substituted Triarylmethyl Radicals, *Inorg. Chem.*, 2015, **54**, 4186–4188; (*c*) Y. Hattori, T. Kusamoto, T. Sato and H. Nishihara, Synergistic luminescence enhancement of a pyridyl-substituted triarylmethyl radical based on fluorine substitution and coordination to gold, *Chem. Commun.*, 2016, **52**, 13393–13396.

11 (*a*) V. Gamero, D. Velasco, S. Latorre, F. López-Calahorra, E. Brillas and L. Juliá, [4-(N-Carbazolyl)-2,6-dichlorophenyl]bis(2,4,6-trichlorophenyl)methyl radical an efficient red light-emitting paramagnetic molecule, *Tetrahedron Lett.*, 2006, **47**, 2305–2309; (*b*) D. Velasco, S. Castellanos, M. López, F. López-Calahorra, E. Brillas and L. Juliá, Red Organic Light-Emitting Radical Adducts of Carbazole and Tris(2,4,6-trichlorotriphenyl)methyl Radical That Exhibit High Thermal Stability and Electrochemical Amphotericity, *J. Org. Chem.*, 2007, **72**, 7523–7532; (*c*) S. Castellanos, D. Velasco, F. López-Calahorra, E. Brillas and L. Juliá, Taking Advantage of the Radical Character of Tris(2,4,6-trichlorophenyl)methyl To Synthesize New Paramagnetic Glassy Molecular Materials, *J. Org. Chem.*, 2008, **73**, 3759–3767; (*d*) S. Dong, W. Xu, H. Guo, W. Yan, M. Zhang and F. Li, Effects of substituents on luminescent efficiency of stable triaryl methyl radicals, *Phys. Chem. Chem. Phys.*, 2018, **20**, 18657–18662; (*e*) A. Heckmann, S. Dümmler, J. Pauli, M. Margraf, J. Köhler, D. Stich, C. Lambert, I. Fischer and U. Resch-Genger, Highly Fluorescent Open-Shell NIR Dyes: The Time-Dependence of Back Electron Transfer in Triarylamine-Perchlorotriphenylmethyl Radicals, *J. Phys. Chem. C*, 2009, **113**, 20958–20966; (*f*) Y. Zhao, A. Abdurahman, Y. Zhang, P. Zhang, M. Zhang and F. Li, Highly Efficient Multifunctional Luminescent Radicals, *CCS Chem.*, 2022, **4**, 722–731; (*g*) R. Xiaotian, W. Ota, T. Sato, M. Furukori, Y. Nakayama, T. Hosokai, E. Hisamura, K. Nakamura, K. Matsuda, K. Nakano, A. P. Monkman and K. Albrecht, Carbazole-Dendronized Luminescent Radicals, *Angew. Chem., Int. Ed.*, 2023, e202302550.

12 Y. Hattori, R. Kitajima, R. Matsuoka, T. Kusamoto, H. Nishihara and K. Uchida, Amplification of luminescence of stable radicals by coordination to NHC–gold(I) complex, *Chem. Commun.*, 2022, **58**, 2560–2563.

13 Y. Hattori, R. Kitajima, W. Ota, R. Matsuoka, T. Kusamoto, T. Sato and K. Uchida, The simplest structure of a stable radical showing high fluorescence efficiency in solution: benzene donors with triarylmethyl radicals, *Chem. Sci.*, 2022, **13**, 13418–13425.

14 S. Mattiello, F. Corsini, S. Mecca, M. Sassi, R. Ruffo, G. Mattioli, Y. Hattori, T. Kusamoto, G. Griffini and L. Beverina, First demonstration of the use of open-shell derivatives as organic luminophores for transparent luminescent solar concentrators, *Mater. Adv.*, 2021, **2**, 7369–7378.

15 (*a*) G. Scalmani and M. J. Frisch, Continuous surface charge polarizable continuum models of solvation. I. General formalism, *J. Chem. Phys.*, 2010, **132**, 114110; (*b*) R. Improta, V. Barone, G. Scalmani and M. J. Frisch, A state-specific polarizable continuum model time dependent density functional theory method for excited state calculations in solution, *J. Chem. Phys.*, 2006, **125**, 054103.

16 (*a*) M. López, D. Velasco, F. López-Calahorra and L. Juliá, Light-emitting persistent radicals for efficient sensor devices of solvent polarity, *Tetrahedron Lett.*, 2008, **49**, 5196–5199; (*b*) L. Fajarí, R. Papoular, M. Reig, E. Brillas, J. L. Jorda, O. Vallcorba, J. Rius, D. Velasco and L. Juliá, Charge Transfer States in Stable Neutral and Oxidized Radical Adducts from Carbazole Derivatives, *J. Org. Chem.*, 2014, **79**, 1771–1777; (*c*) Y. Hattori, E. Michail, A. Schmiedel, M. Moos, M. Holzapfel, I. Krummenacher, H. Braunschweig, U. Meller, J. Pflaum and C. Lambert, Luminescent Mono-, Di-, and Triradicals: Bridging Polychlorinated Triarylmethyl Radicals by Triarylamines and Triarylboranes, *Chem. – Eur. J.*, 2019,

 © 2023 The Author(s). Published by the Royal Society of Chemistry

Open Access Article. Published on 26 September 2023. Downloaded on 12/4/2025 9:20:33 PM.
This article is licensed under a Creative Commons Attribution-NonCommercial 3.0 Unported Licence.

25, 15463–15471; (*d*) S. Mattiello, Y. Hattori, R. Kitajima, R. Matsuoka, T. Kusamoto, K. Uchida and L. Beverina, Enhancement of fluorescence and photostability of luminescent radicals by quadruple addition of phenyl groups, *J. Mater. Chem. C*, 2022, **10**, 15028–15034.

17 K. Matsuda, R. Xiaotian, K. Nakamura, M. Furukori, T. Hosokai, K. Anraku, K. Nakao and K. Albrecht, Photostability of luminescent tris(2,4,6-trichlorophenyl)methyl radical enhanced by terminal modification of carbazole donor, *Chem. Commun.*, 2022, **58**, 13443–13446.